Effect of temperature and thermal cycling on fatigue crack growth in aluminium reinforced with GLARE bonded crack retarders

Syed, A, Zhang, X, Moffatt, JE & Fitzpatrick, ME

Original citation & hyperlink:
Syed, A, Zhang, X, Moffatt, JE & Fitzpatrick, ME 2017, 'Effect of temperature and thermal cycling on fatigue crack growth in aluminium reinforced with GLARE bonded crack retarders' *International Journal of Fatigue*, vol 98, pp. 53-61
https://dx.doi.org/10.1016/j.ijfatigue.2017.01.018

DOI 10.1016/j.ijfatigue.2017.01.018
ISSN 0142-1123

Publisher: Elsevier

Accepted Manuscript

Effect of temperature and thermal cycling on fatigue crack growth in aluminium reinforced with GLARE bonded crack retarders

Abdul Khadar Syed, Xiang Zhang, James E. Moffatt, Michael E. Fitzpatrick

PII: S0142-1123(17)30018-X
DOI: http://dx.doi.org/10.1016/j.ijfatigue.2017.01.018
Reference: JIJF 4208

To appear in: *International Journal of Fatigue*

Received Date: 26 October 2016
Revised Date: 10 January 2017
Accepted Date: 11 January 2017

Please cite this article as: Syed, A.K., Zhang, X., Moffatt, J.E., Fitzpatrick, M.E., Effect of temperature and thermal cycling on fatigue crack growth in aluminium reinforced with GLARE bonded crack retarders, *International Journal of Fatigue* (2017), doi: http://dx.doi.org/10.1016/j.ijfatigue.2017.01.018

Effect of temperature and thermal cycling on fatigue crack growth in aluminium reinforced with GLARE bonded crack retarders

Abdul Khadar Syed[1,2 *], Xiang Zhang[1], James E. Moffatt[2], Michael E. Fitzpatrick[1]

[1] Faculty of Engineering, Environment and Computing, Coventry University, Priory Street, Coventry CV1 5FB, UK

[2] Materials Engineering, The Open University, Walton Hall, Milton Keynes MK7 6AA, UK

*Corresponding author; Email address: abdul.syed@coventry.ac.uk (AK Syed), xiang.zhang@coventry.ac.uk (X Zhang); michael.fitzpatrick@coventry.ac.uk (ME Fitzpatrick)

Abstract

This paper presents results of fatigue crack growth testing of aluminium alloy 2624-T351 reinforced by bonded crack retarders made of GLARE fibre-metal laminate. Specimens were tested at room temperature, 70°C and −60°C. Better performance of the crack retarders in terms of increased fatigue life was achieved at room temperature than at the two temperature extremes. This is attributed to a combined effect of change in the fatigue crack growth rate at temperature in the substrate material, and residual stress generated at temperatures above or below room temperature. The change in fatigue crack growth rate was measured, and the substrate deformation and the stress intensity factors at temperature were calculated by Finite Element Analysis. In addition, the effect of thermal load cycling on fatigue crack growth rate was investigated by exposing the specimens to repeated thermal cycles between 70°C and –60°C prior to fatigue

testing. It is concluded that the pre-test thermal cycling has little effect on the fatigue crack growth rate.

Keywords: Aluminium alloys, Bonded crack retarders, , crack growth rate, Fatigue crack growth, Thermal cycling

Highlights

- GLARE straps provided considerable reduction to FCG rate at RT.
- At −60°C, baseline FCG life is more than tripled owing to the reduced FCG rate.
- At 70°C, baseline FCG life is shorter owing to greater stress intensity factors.
- Thermal cycling does not impair the performance of BCR tested at RT.

1. Introduction

The continuing increase in demand for air transportation requires new design concepts to achieve lightweight, low-operating-cost aircraft structures. Novel manufacturing technologies have led to the development of integral metallic structures to replace the conventional built-up structures containing riveted joints. Integral structures potentially reduce the structural weight and manufacturing cost. A major concern in using integral structures is the reduced resistance to fatigue crack growth (FCG) owing to the lack of inherent crack-stoppers. Regulatory authorities require such structures to utilise additional design features to ensure fail safety and damage tolerance. Bonded crack retarder (BCR) technology has been developed to improve the fatigue performance of integral metallic structures. Reinforcing straps are adhesively bonded on to the structure at the manufacture stage, in locations where crack propagation is expected. The local increase in stiffness, coupled with the crack-bridging capability of the strap, reduce the crack growth driving force thereby reducing the crack growth rates [1, 2].

Use of adhesively bonded repair of aluminium structures with composite or metal patches has received a lot of attention [3-9]. Previous studies have shown that the reinforcing strap material incompatibility with the substrate resulted in significant residual stresses, material failure and galvanic corrosion problems [6, 7]. In recent years, the GLARE fibre-metal laminate system has been identified as the most promising material for BCR [10, 11] owing to its low weight and excellent fatigue performance, and also compatibility with the aluminium substrate [11]. GLARE consists of alternating layers of thin aluminium sheet and glass-fibre-reinforced epoxy. Although BCR technology improves the fatigue performance of the reinforced structure, potential concerns are the development of thermal residual stress, the integrity of the bond interface under fatigue loading, and the consequences of any out-of-plane deformation following the strap bonding process.

The elevated temperature curing of the adhesive used during the BCR bonding process will produce tensile residual stresses in the aluminium substrate owing to the difference in the coefficient of thermal expansion (CTE) between the substrate and strap materials [12]. At the curing temperature, there will be zero residual stress present. After the bond is cured and cooled down to room temperature, tensile residual stresses will develop in the substrate. The magnitude of the residual stress depends on the mismatch between the CTE and elastic modulus of the substrate and strap, the (relative) thicknesses, and the curing temperature. Tensile residual stresses present in the substrate structure will add to the service loads and may result in a significant change in the stress intensity factor of a growing crack, thereby reducing the potential fatigue life improvement [12, 13]. Previous work has shown that curing GLARE straps at elevated temperature introduces relatively low residual stresses and should not impair the

benefits of the crack retarder [12-14]. Therefore, GLARE has been selected for further studies of the performance of BCR under service conditions.

During service, aircraft structures are exposed to a range of operating temperatures, from up to 70°C on the ground to −60°C at cruise altitudes. Research performed in [15] investigated the magnitude of residual stresses caused by bonded titanium straps at room temperature (RT) and −50°C, and found that the peak residual stress in the substrate had doubled at −50°C compared to that at RT.

To the authors' knowledge there is no previous work investigating the effect of temperature and thermal cycling on the fatigue crack growth performance of aluminium reinforced by bonded GLARE straps. To address these research questions, two different tests have been conducted on aluminium 2624-T351 plate reinforced by GLARE straps, to investigate: (a) fatigue crack growth rates at RT, 70°C and −60°C; and (b) effect of prior thermal cycling on the fatigue crack growth rate at RT. Thermal cycling was performed between –60°C and 70°C, followed by room temperature fatigue crack growth testing.

2. Experimental details

2.1. Materials and test specimens

Middle-crack Tension (M(T)) specimens were prepared from aluminium alloy 2624-T351 plate with dimensions 400 × 140 × 5 mm^3. Figure 1 shows the geometry and dimensions of the M(T) specimen bonded with a pair of GLARE straps. A crack starter notch of 16 mm was introduced in the M(T) specimens using the electro-discharge machining process. Experiments were performed on the specimens with and without GLARE straps. One important parameter that contributes to the performance of the BCR is the global stiffness ratio (μ), which is defined as [16]:

$$\mu = \frac{\sum(E_{strap} \cdot A_{strap})}{(E_{Al} \cdot A_{Al}) + \sum(E_{strap} \cdot A_{strap})} \quad (1)$$

where E_{strap}, E_{Al} and A_{strap}, A_{Al} are the elastic modulus and cross-section area of the straps and the substrate material respectively.

In this study, a global stiffness ratio of 0.2 was chosen and GLARE 2A-6/5 was selected as the crack retarder material, which consists of six layers of aluminium alloy sheets (each 0.4-mm-thick) and five layers of unidirectional glass-fibre-reinforced epoxy (each 0.26-mm-thick). The dimensions of the strap were 180 mm in length, 25.83 mm width and 3.7 mm thickness. Glass fibres in GLARE are oriented along the longitudinal direction (X-direction in Figure 1). The mechanical properties of GLARE 2 (6/5) in the fibre direction are tensile modulus = 64 GPa, ultimate tensile strength = 1091 MPa, and tensile yield strength = 331 MPa.

Table 1 shows the mechanical properties of the substrate and adhesive used in this investigation. The substrate and strap assembly was bonded using Cytec FM94® adhesive [17]. The curing temperature of the adhesive was 120°C and the curing procedure is described in detail in [14]. After the curing, specimens were inspected using an ultrasonic phased array C-scan to confirm the bond quality. The stated operating temperature range for the adhesive in [17] is −55 to 104°C. Therefore, the lowest test temperature is slightly outside this range; however, the property limits for the adhesive are at the upper end of the temperature range rather than the lower.

2.2. Measurement of out-of-plane deformation

The specimens were subjected to in-plane loading in fatigue tests with loading along the longitudinal direction (the X-direction, see figure 1). Owing to the asymmetric strap configuration (straps were bonded on one side of the plate only), out-of-plane

deformation will occur after the curing of the straps, and additionally during the fatigue loading because of the secondary bending effect (see figure 3).

Following curing of the crack retarders at elevated temperature residual stresses exist owing to the mismatch of the elastic modulus and coefficient of thermal expansion between the aluminium substrate and the GLARE straps. Because of the asymmetric strap configuration, these residual stresses will cause out-of-plane deformation. This deflection was measured on the specimens after the strap bonding process using a co-ordinate measurement machine. The measurement was performed on the unreinforced (back) side along the specimen longitudinal direction with a 1 mm measurement interval.

Secondly, single-sided strap arrangement causes a shift in the neutral axis in the specimen, resulting in so-called secondary bending when an in-plane load is applied. To evaluate the magnitude of the secondary bending at the maximum applied load of the test, a pair of strain gauges was attached to a specimen. Strain measurements were performed at room temperature as the sample was loaded. As shown in Figure 1, the strain gauges were positioned on both sides of the specimen at a position remote from the crack tip stress concentration and on the horizontal centre line, at a distance of 60 mm from the centre of the specimen. A static load of 53.4 kN (resulting in 60 MPa nominal applied stress in the far-field of the plate) was applied under displacement control of 0.1 mm/min. The strain data on both reinforced and unreinforced side were recorded, and used to validate the FE model that is presented in Section 3.

2.3. Fatigue crack growth testing at temperature

The efficacy of the bonded crack retarder was investigated by at-temperature constant-amplitude tension-tension fatigue crack growth testing on specimens with and without

straps. Table 2 summarises the results. Fatigue crack growth tests were performed using a 100 kN MTS servo-hydraulic test machine. Specimens were subjected to a maximum applied stress of 60 MPa with a stress ratio of 0.1 and at 10 Hz loading frequency. Crack length measurement was performed on the unreinforced side with a travelling microscope with a 7× objective magnification and an accuracy of ± 0.01 mm. Tests were performed according to the ASTM E 647-15e1 standard [18]. For tests at −60°C and 70°C, an Instron 3119-407 environmental chamber was used and the specimens were coupled with an N-type thermocouple to monitor the temperature with an accuracy of ±0.5°C. For tests at −60°C, liquid nitrogen was used as a cooling medium.

2.4. Pre-fatigue thermal cycling

Twelve specimens were thermal cycled between the minimum temperature −60°C to the maximum temperature 70°C using a VOTSCH (VTS 7010) thermal cycling chamber. Each specimen was coupled with an N-type thermocouple to record the temperature with an accuracy of ±0.5°C. After reaching the desired temperature, a holding time of 40 minutes was maintained to allow the specimens to equilibrate. After completing a defined number of thermal cycles 500, 1000, 1500, 2000, 3000, and 4500 specimens were removed from the thermal cycling chamber. Two specimens from each thermal cycle history were subsequently tested at constant amplitude load (maximum stress of 60 MPa and stress ratio 0.1) at room temperature using the 100 kN MTS servo-hydraulic test machine.

3. Finite Element modelling

Finite element modelling was carried out using the commercial software package ABAQUS. Linear elastic material properties in Table 1 were used for the analysis. Figure 2 shows a full-scale specimen as modelled. The aluminium substrate, adhesive

layer, and straps were modelled using 8-noded continuum brick elements with reduced integration (designated in ABAQUS as C3D8R). Following a mesh convergence study, element sizes of $1 \times 1 \times 1$ mm^3, and a finer mesh of $0.5 \times 0.5 \times 0.5$ mm^3 along the crack path in the substrate were used. The substrate-adhesive and adhesive-strap interfaces were modelled by surface- based constraints. The degrees of freedom on the slave surface are eliminated and the nodes are set to deform with the closest node on the master surface using the ABAQUS TIE option. Thermal residual stresses owing to curing at 120°C are inputted in the model prior to the applied stress. In accordance with the method in [12], work thermal residual stresses (~20MPa) were inputted into the model via a predefined field. During the FE analysis, the specimen is subjected to a far-field tensile stress of 60 MPa or 6 MPa (representing the maximum and minimum stresses during the fatigue crack growth testing) and subjected to room temperature, 70°C and −60°C. During the 70°C and −60°C analysis, the temperature was applied on whole M(T) assembly by using the respective thermal boundary conditions.

4. Results and discussion

4.1. Out-of-plane deformation after strap bonding

After curing the adhesive at 120°C, out-of-plane deformation was observed at room temperature owing to the asymmetric configuration of the strap-reinforced specimens. Figure 3a shows the measured out-of-plane deformation resulting from the bonding process, and Figure 3b is a schematic of the specimen deformation before and after the strap bonding process. The maximum deformation is 0.9 mm, which is 18% of the substrate thickness.

4.2. Secondary bending at the maximum fatigue load

Strain measurement was conducted on a reinforced specimen at the maximum applied stress of 60 MPa (53.4 kN load) during static loading, as described in section 2.2. Owing to the secondary bending effect, there is a significant difference in strains between the reinforced and unreinforced sides of the substrate (measured at the gauge positions in Figure 1). At the maximum applied load, the strain on the unreinforced side is 1200 με, and 700 με on the strap side. Therefore, the bending strain is 250 με, i.e. (1200–700) / 2. Using the Young's modulus of 71 GPa, the bending stress is about 17 MPa acting on the unreinforced side of the substrate (i.e. 28% of the maximum applied stress during the testing).

4.3. Fatigue crack growth rates at temperature

Figure 4 shows the average half crack length versus number of cycles at the three test temperatures, for specimens with and without bonded straps. At room temperature, the strap-reinforced specimens show an average life improvement factor of 1.27 compared to the unreinforced specimens.

Elevated temperature (70°C) resulted in shorter fatigue life both in unreinforced and reinforced condition and resulted negligible benefit of the BCR.. At low temperature (−60°C), longer life than the specimens tested at room temperature was seen, by a factor of ~3, but overall there is.no clear benefit of the BCR on the fatigue life.

Figure 5 shows the crack growth rate (da/dN) vs. half crack length with and without straps. At RT, there is a noticeable difference in the slope of the crack growth rate curve of with-strap specimens compared to without-strap: the crack growth rate becomes slower when the crack propagates under the strap ($a < 40$ mm). At 70°C (Fig

5a) crack growth rate is increased compared to RT and there is no difference between the with-strap and without-strap cases. At −60°C (Figure 5b) a significant decrease in crack growth rate is seen compared to the RT tests.

The difference in fatigue crack growth rates between the reinforced and unreinforced specimens tested at RT, 70°C and −60°C may be attributed to two factors. First, the change in the substrate material's intrinsic fatigue crack growth rate properties at different temperatures. Second, the temperature will affect the residual stresses in the substrate, which leads to a change in the effective or total stress intensity factor that is the crack growth driving force. To verify the first factor, fatigue crack growth rate is plotted against to the applied stress intensity factor range (ΔK) for the unreinforced specimens, in figure 6, at the three different temperature values.

$$\Delta K = \beta\ (\sigma_{max}\ - \sigma_{min})\sqrt{\pi a}) \qquad (2)$$

Where $\sigma_{\max}$ and $\sigma_{\min}$ are maximum and minimum applied stress, a is crack length and β is geometry factor.

Figure 6 shows that for a given ΔK_{app}, da/dN at −60°C is significantly lower than at room temperature (by an order of magnitude). In the Paris law, da/dN = C $(\Delta K)^n$,: the material constants C and n are dependent on the testing conditions, such as the load ratio R, test temperature and humidity. The experimentally-measured C and n values for unreinforced specimens at RT, 70°C and −60°C are deduced by a curve fit in the Paris law region of the da/dN vs ΔK data and given in Table 3. It is clear that the n values for the three temperatures are comparable, but C for −60°C is an order of magnitude lower. This is the reason why specimens tested at −60°C have significantly longer fatigue life compared to the RT and 70°C tests.

In addition, the maximum stress intensity factor K_{max} also changes owing to residual stresses at-temperature. This is discussed in Section 4.4. To account for this effect, either the effective R-ratio, or K_{max} can be used in a two-parameter fatigue crack growth rate law, e.g. the Forman or Walker equations [19].

4.4. FE analysis

FE results of the substrate deformation owing to thermal residual stresses after curing the adhesive are shown in figure 7b, which is in good agreement with the experimental measurement. Owing to the geometric asymmetry, the out-of-plane deformation will change when the specimen is under fatigue loading and exposed to test temperatures. To investigate this effect further, FE analysis was carried simulating loading of 6 MPa and 60 MPa stress applied in the longitudinal direction at RT, 70°C and −60°C temperatures during the analysis. The schematic of the specimen deformation after loading at three temperatures and the FE calculated deformation after curing, at 6 MPa and 60 MPa are shown in figures 7b-7d respectively.

Deformation after curing (at zero load)

After cure, the sample is deformed by a maximum of 0.9 mm owing to the cure temperature effect (z = −0.9 mm, for coordinate definition refer to figure 1). Figure 7b shows FE and experimental results of specimen deformation after adhesive curing. The FE and the experimental results are in good agreement.

Deformation at 6 MPa

Figure 7c shows the specimen deformation at 6 MPa. Note that this is a low load and the deformation is therefore caused predominantly by the CTE mismatch. At room temperature the specimen did not change its initial deformation shape and there is little change in deformation magnitude (z = −0.7 mm). At 70°C the specimen is deformed in

the opposite direction (z = +2.28 mm) to that of the post-curing deformation with significant difference in the magnitude compared to the post-cure deformation. This is due to the difference in CTE between the substrate and the adhesive. At −60°C there was also significant change in the deformation magnitude compared to that after cure, resulting in a deformation of z = −3.29 mm. This significant deformation at small applied stress is again attributed to the CTE difference between the substrate and the adhesive at −60°C.

Deformation at 60 MPa

Figure 7d shows the specimen out-of-plane deformation at 60 MPa applied stress. At RT and 70°C, the specimen is deformed in the opposite direction to that of the curing deformation with z = +1.04 mm (RT) and 4.07 mm (70°C) from the unreinforced side. In contrast, at −60°C the specimen retains the initial deformation shape with a larger magnitude of z = −1.34 mm. This difference is due to a combination of the asymmetric strap bonding and the CTE difference between the substrate and strap. After strap bonding, with no external load, specimen deformation results in compressive [8] and tensile stresses on the unreinforced and reinforced side respectively. However, at RT, and at 70°C with loading of 60 MPa, the deformation is reversed giving tensile stresses on the unreinforced side that accelerate fatigue crack growth on that side. Owing to the much larger deformation at 70°C compared to RT, the magnitude of the tensile stresses is higher at 70°C; hence a greater crack growth rate. On the other hand, the increase in magnitude of deformation at −60°C resulted in less tension on the unreinforced side, which reduces the fatigue crack growth rate hence giving longer crack growth life compared to RT and 70°C. It should be noted that these effects are a consequence of the

particular geometry of the samples studied here and the associated constraint, and that different results may be obtained for different configurations.

These significant changes in deformation on loading will result in variation in stresses and stress intensity factors through the specimen thickness. To investigate this further, a specific case of an 11-mm-half crack subjected to 60 MPa and 6 MPa applied stress at RT, 70°C and −60°C was modelled. Figure 8 shows the stress distribution on the two sides of the specimen. Owing to the out-of-plane deformation at the maximum applied stress of 60 MPa (figure 7a, 7b), the crack tip stress is much higher at the unreinforced side for the RT and 70°C tests, whereas the peak stress location reverses for the −60°C case, i.e. the peak stress is on the reinforced side.

Figure 9a shows the through-thickness distribution of the maximum total stress intensity factor (K_{max}) at applied stress of 60 MPa and the three temperature values. From figure 9a, the following observations can be made:

1) On the unreinforced side, at RT and 70°C the specimens have higher K on the unreinforced side whereas at−60°C the unreinforced side has lower K.
2) At RT, the K variation through the substrate thickness is small, and higher K on the unreinforced side promotes faster crack growth compared to the reinforced side. At 70°C, the K variation through the substrate thickness is significant (14 MPa√m) owing to the larger secondary bending. Higher K on the unreinforced side promotes faster crack growth rate compared to the reinforced side.
3) At −60°C, there is lower K on the unreinforced side with a variation of 4 MPa√m through the substrate thickness. The lower K on the unreinforced side is due to reversed secondary bending, causing much reduced fatigue crack growth rate; hence longer fatigue life as measured experimentally (Figure 4).

FE calculated K values corresponding to the minimum applied stress of 6 MPa are shown in figure 9b. In this case, at RT the specimen shows lower K on the unreinforced than the reinforced side, indicating that the minimum applied stress does not affect the substrate deformation (refer to figure 7c). At 70°C, K is higher on the unreinforced side and reduces to zero from 2 mm below the back face (see figure 9b). It was observed during the FE analysis for the specimen subjected to 6 MPa at 70°C that the crack is not fully opened on the reinforced side (owing to secondary bending, and residual stresses) whereas it is fully opened on the unreinforced side. Similar behaviour is also observed at −60°C with the crack not fully opened on the unreinforced side. This indicates that the thermal residual stresses in the substrate have resulted in partial crack closure on the unreinforced side of the specimens at −60°C.

The stress intensity factor range governs fatigue crack growth rate. Since the experimental crack growth measurements were recorded only on the unreinforced side, ΔK values on this side are used for the analysis. Taking a = 11 mm for example: $\Delta K = K_{max} - K_{min}$ values are 11.4, 11.4 and 9.7 MPa√m at RT, 70°C and −60°C, respectively. This partially explains the much slower crack growth rate at −60°C compared to the RT and 70°C tests as presented in Figure. 5. The main reason for the much slower crack growth rate at −60°C is the material's crack growth properties as shown in Figure.6 and Table 3. Although the ΔK values on the unreinforced side for RT and 70°C are similar, at 70°C the specimen shows faster crack growth rate compared to RT: Figure.5 clearly shows higher fatigue crack growth rate at 70°C when ΔK = 15-20 MPa√m.

4.5. Strap delamination and fracture surfaces

Another key parameter determining the BCR performance in terms of the fatigue crack growth life or crack growth rate is the strap delamination behaviour during fatigue. Two types of strap delamination were observed in the tests: (i) delamination between the substrate and the strap (i.e. cohesive failure in the adhesive); and (ii) delamination within the strap i.e. delamination propagation in the first interface within the GLARE (the interface closest to the bond with the substrate). The type of delamination depends on several parameters, such as the degree of secondary bending and residual stresses in the reinforced structure. The area of delamination will influence the performance of the bonded crack retarder.

In this work all the specimens tested at RT and 70°C showed debonding failure in the adhesive layer i.e. cohesive damage. Figure 10 shows images of the post-failure specimen tested at 70°C. Since the crack tip stress is very low on the reinforced side owing to bending (Figure. 8), this debonding damage is thought to be triggered by the moving crack tip.

Specimens tested at −60°C showed delamination damage running through the first layer of the GLARE, as shown in figure 11. This is owing to the increase in thermal residual stresses and total stress at the reinforced side (Figure. 8). This causes delamination between the first aluminium layer and the glass fibre ply of the GLARE strap. Further cyclic loading of the specimen results in delamination propagation within the GLARE strap.

4.6. Effect of thermal cycling prior to fatigue testing

Figure 12 shows fatigue crack propagation life at RT for specimens thermal cycled prior to fatigue tests. Specimens were thermal cycled between −60°C and 70°C and then

removed from the thermal chamber and subjected to RT fatigue tests as described in Section 2.

Two tests were performed for each case and Table 4 shows the average fatigue life. It can be seen that thermal cycling up to 4500 cycles does not have a negative effect on the crack growth life: in fact, above 1500 thermal cycles the lives are actually longer, but this is not likely to be systematic. The overall scatter in the data is no more than 10%, which is well within the variability range given the inherent scatter in the fatigue damage process and changes in laboratory temperature and humidity conditions during the test programme.

In summary, the thermal cycling has no measurable effect on the fatigue performance of the bonded crack retarders. There is no degradation of the properties of any of the components of the assembly resulting from exposure to the temperature extremes defined for the programme.

Conclusions

A middle-crack tension M(T) geometry made of aluminium alloy 2624-T351 reinforced with GLARE bonded crack retarders was tested at room temperature (RT), 70°C and −60°C. The effect of prior thermal cycling on fatigue crack growth at RT was also investigated. Finite element analysis was conducted to aid understanding of the test results. The straps were bonded to one side of the substrate only, as would be the case in the majority of target application. The following conclusions can be drawn.

1. The single-side strap configuration used and the residual stress arising from curing of the adhesive at elevated temperature cause out-of-plane deformation. In this study, the maximum deformation is 0.9 mm.

2. Secondary bending occurs when applying in-plane loading during the fatigue testing. The bending direction and its magnitude depend on the test temperature, The consequent stress variation affects the stress intensity factor to different degrees on both sides of the specimen; and consequently, the crack growth rate.
3. At room temperature, fatigue crack growth life was increased by 27% owing to the bonded straps. Note that the 2624 alloy has high damage tolerance, and this (coupled with the specimen design and stiffness ratio) leads to an improvement that is relatively modest compared to those seen in some previous work.
4. At 70°C, straps brought little improvement on crack growth life. This is attributed to the increased residual stress, secondary bending, and greater stress intensity factor. Specimens tested at room temperature and 70°C showed cohesive failure at the adhesive layer.
5. The –60°C tests also showed little improvement on crack growth life. This is partly a consequence of the much reduced fatigue crack growth rate at –60°C (with and without straps), and much reduced residual stress and reversed secondary bending. At –60°C, delamination failure was found within the GLARE strap.
6. Thermal cycling prior to fatigue testing at room temperature does not impair the performance of the bonded crack retarders.

Acknowledgements

The authors would like to thank all the participants involved in this project including Alcoa, and Canfield University. MEF is grateful for funding from the Lloyd's Register Foundation, a charitable foundation helping to protect life and property by supporting engineering-related education, public engagement and the application of research.

References

1. Heinimann M, Bucci R, Kulak M, Garratt M. Improving damage tolerance of aircraft structures through the use of selective reinforcement. Proceedings of the 23rd symposium of International Committee on Aeronautical Fatigue, ICAF 2005, Hamburg, June 2005: 197–208.
2. Zhang X, Boscolo M, Figueroa-Gordon D, Allegri G, Irving PE. Fail-safe design of integral metallic aircraft structures reinforced by bonded crack retarders. Engineering Fracture Mechanics 2009; 76: 114–133.
3. Klug JC, Sun CT, Large deflection effects of cracked aluminium plates repaired with bonded composite patches. Composite Structures 1998; 42: 291-296.
4. Sabelkin V, Mall S, Avram JB, Fatigue crack growth analysis of stiffened cracked panel repaired with bonded composite patch, Engineering Fracture Mechanics 2006; 73(11):1553-1567.
5. Seo DC, Lee JJ, Fatigue crack growth behavior of cracked aluminum plate repaired with composite patch, Composite Structures 2002 ; 57(1-4): 323-330.
6. Vogelesang LB, Vlot A. Development of fibre metal laminates for advanced aerospace structures, Journal of Materials Processing Technology 2000; 103 (1): 1-5.
7. Sinmazçelik T, Avcu E, Bora MÖ, and Çoban O, A review: Fibre metal laminates, background, bonding types and applied test methods, Materials and Design 2011; 32 (7): 3671–3685.
8. Chukwujekwu Okafor A, Navdeep Singh, Enemuoh UE, Rao SV. Design, analysis and performance of adhesively bonded composite patch repair of cracked aluminum aircraft panels. Composite structures 2005; 71: 258-270.

9. Ouinas D, Bouiadjra BB, Serier B. The effects of disbonds on the stress intensity factor of aluminium panels repaired using composite materials. Composite Structures 2007; 78: 278–284.

10. Boscolo M, Zhang X. A modelling technique for calculating stress intensity factors for structures reinforced by bonded strap, Part 2: validation. Engineering Fracture Mechanics 2010, 77:896–907.

11. Irving PE, Zhang X, Doucet J, Figueroa-Gordon D, Boscolo M, Heinimann M, Shepherd G, Fitzpatrick ME, Liljedahl D. Life extension techniques for aircraft structures – Extending Durability and Promoting Damage Tolerance through Bonded Crack Retarders, ICAF, 2011: 753–770.

12. Liljedahl CDM, Fitzpatrick ME, Edwards L. Residual stresses in structures reinforced with adhesively bonded straps designed to retard fatigue crack growth. Composite Structures 2008; 86: 344–355.

13. Syed AK, Fitzpatrick ME, Moffatt JE. Evolution of residual stress during fatigue crack growth in an aluminium specimen with a bonded crack retarder. Composite Structures 2014; 117: 12–16.

14. Abdul Khadar Syed, Michael E. Fitzpatrick James E. Moffatt, Jeremy Doucet, Isidro Durazo-Cardenas. Effect of impact damage on fatigue performance of structures reinforced with GLARE bonded crack retarders. International Journal of Fatigue 2015; 80; 231–237.

15. Liljedahl C, Fitzpatrick M, Zanellato O, Edwards L. Effect of Temperature on the Residual Stresses in an Integral Structure with a Crack Retarding Patch. Strain 2011:47 (2) 293–298.

16. Schijve J. Crack stoppers and ARALL laminates. Engineering Fracture Mechanics 1990; 37; 405-421.

17. http://www.cytec.com/sites/default/files/datasheets/FM_94982015.pdf. Accessed on 1st August 2016.

18. ASTM E647-15e1,Standard test method for measurement of fatigue crack growth rates. ASTM International 2015.

19. Walker K. The effect of stress ratio during crack propagation and fatigue for 2024-T3 and 7075-T6 aluminum. ASTM STP 462, American Society for Testing and Materials, Philadelphia, PA, 1970; 1–14.

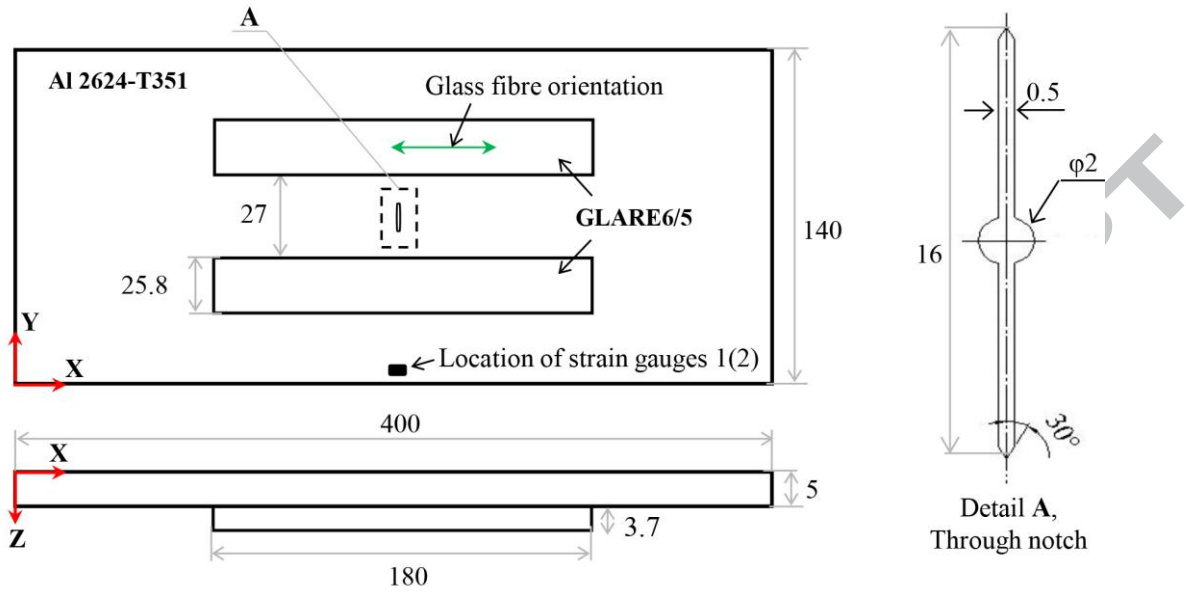

Figure 1: Geometry and dimension of the M(T) specimen with GLARE bonded crack retarders and the strain gauge locations (strain gauge No.2 on back side). Units: mm.

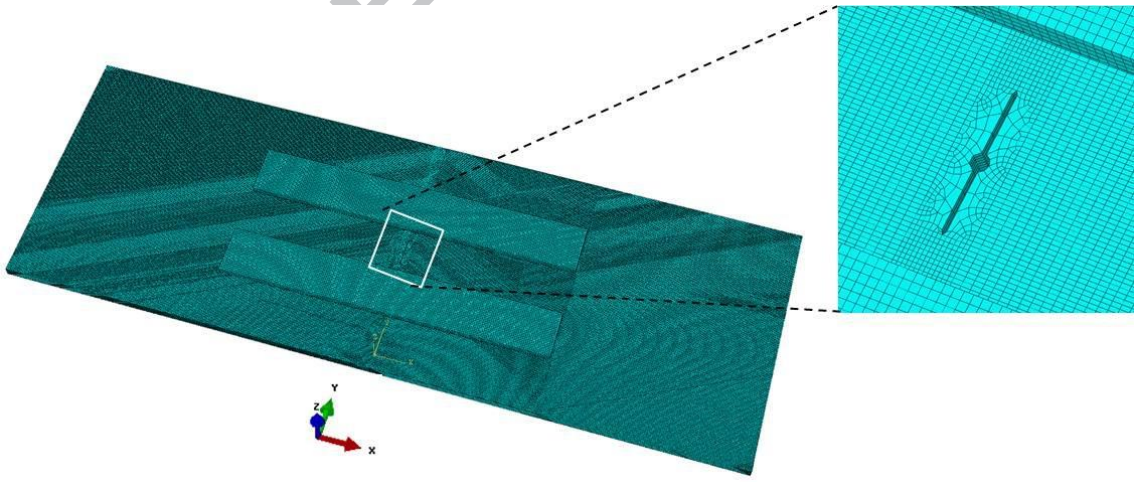

Figure 2: FE model of the M(T) specimen with bonded straps.

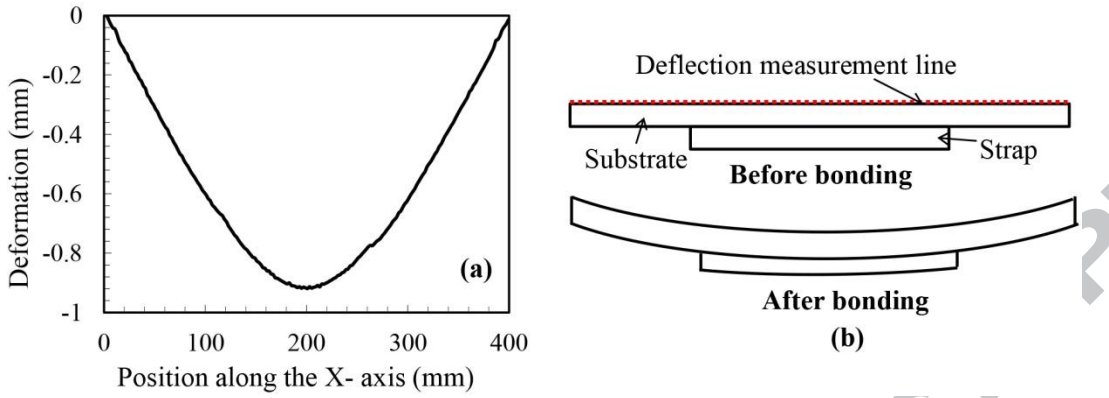

Figure 3: (a) Measured out-of-plane deformation of the M(T) specimen after bonding the GLARE straps, (b) sketch of specimen deformation before and after strap bonding.

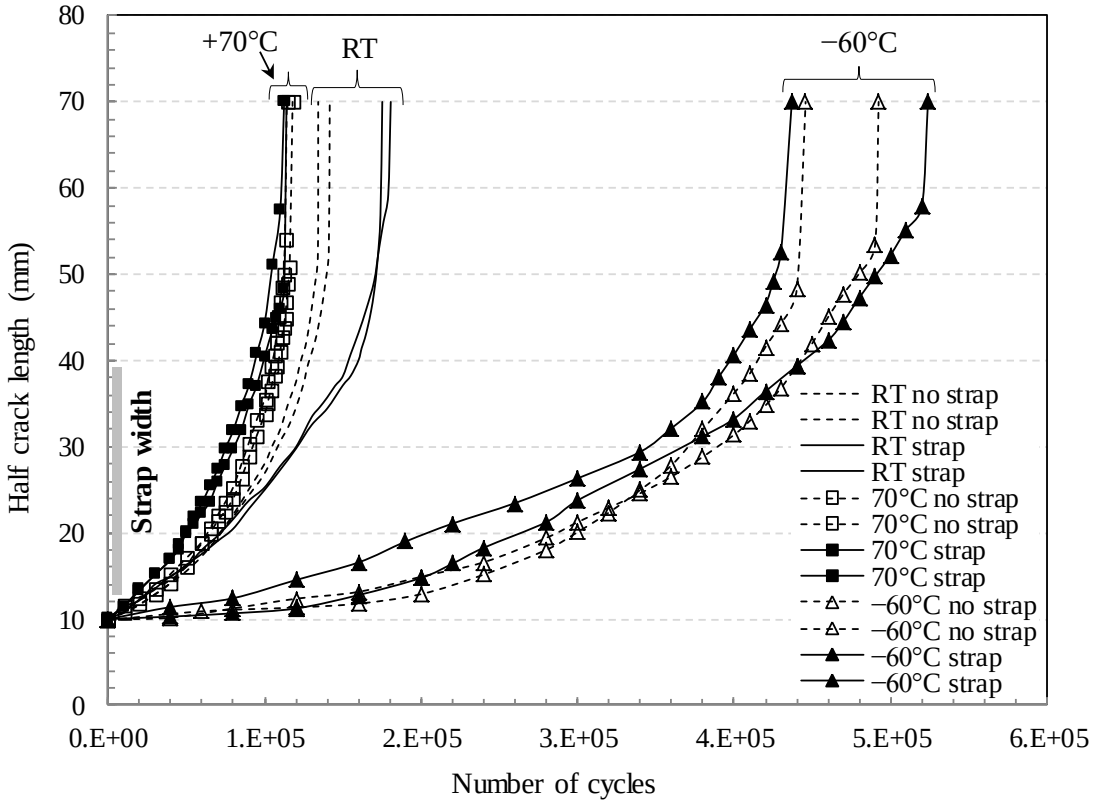

Figure 4: Crack length vs Number of load cycles for specimens with and without bonded crack retarders.

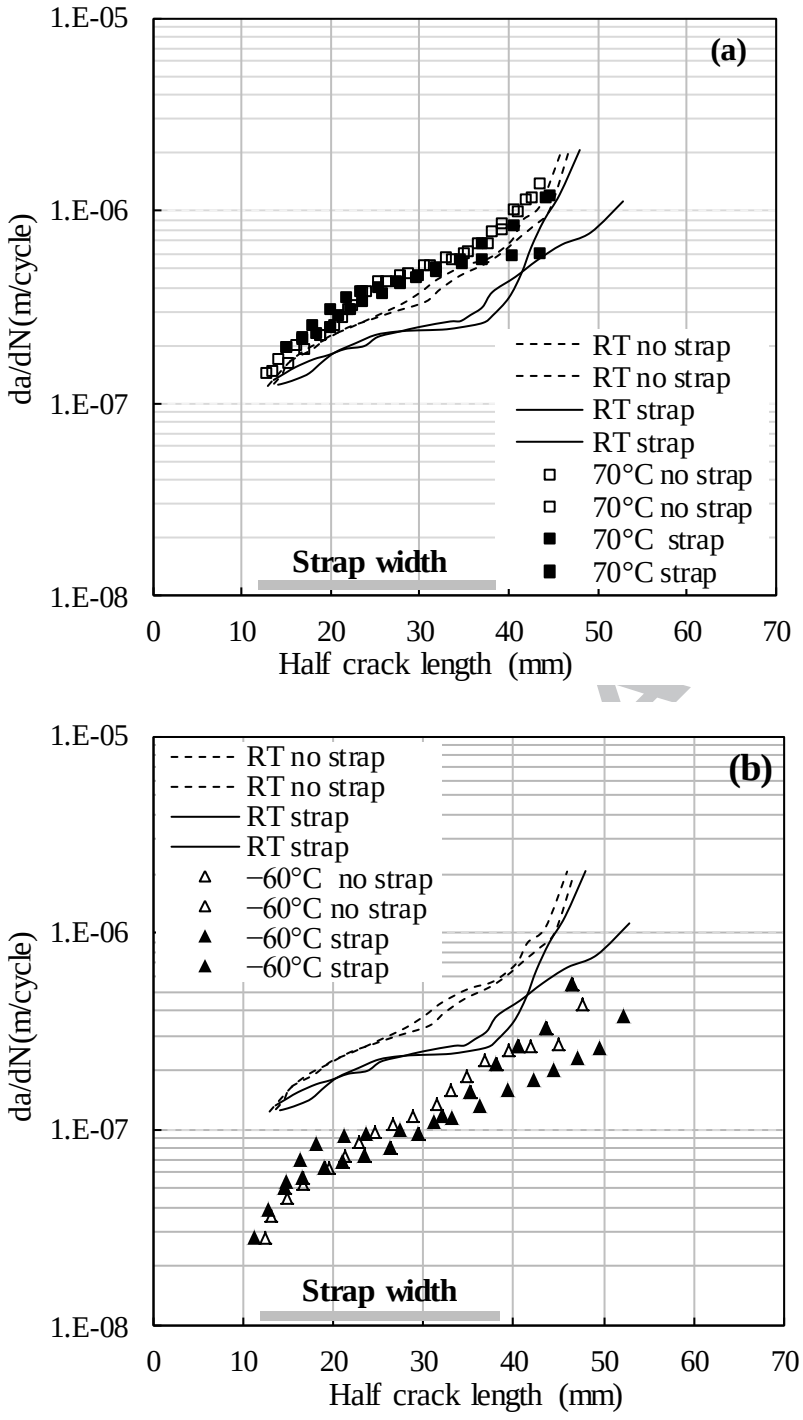

Figure 5: Fatigue crack growth rate vs crack length for (a) RT and 70°C, (b) RT and −60°C tests.

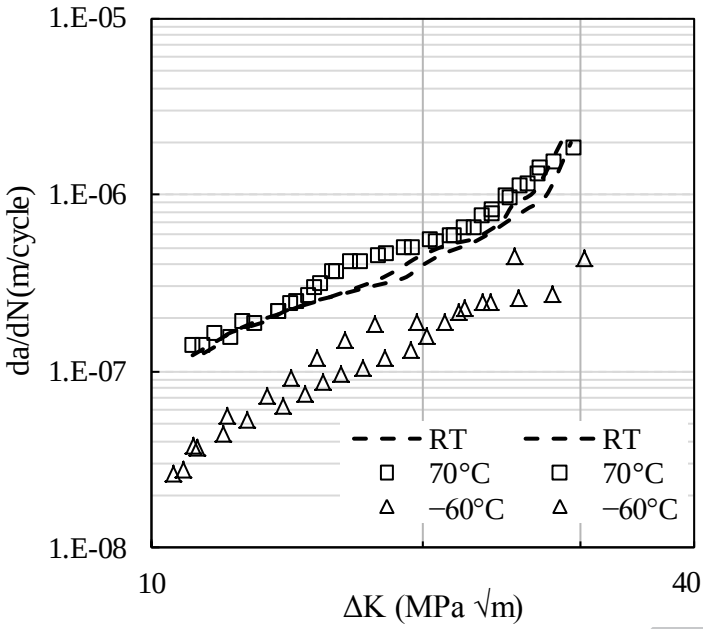

Figure 6: da/dN vs ΔK for unreinforced M(T) specimens.

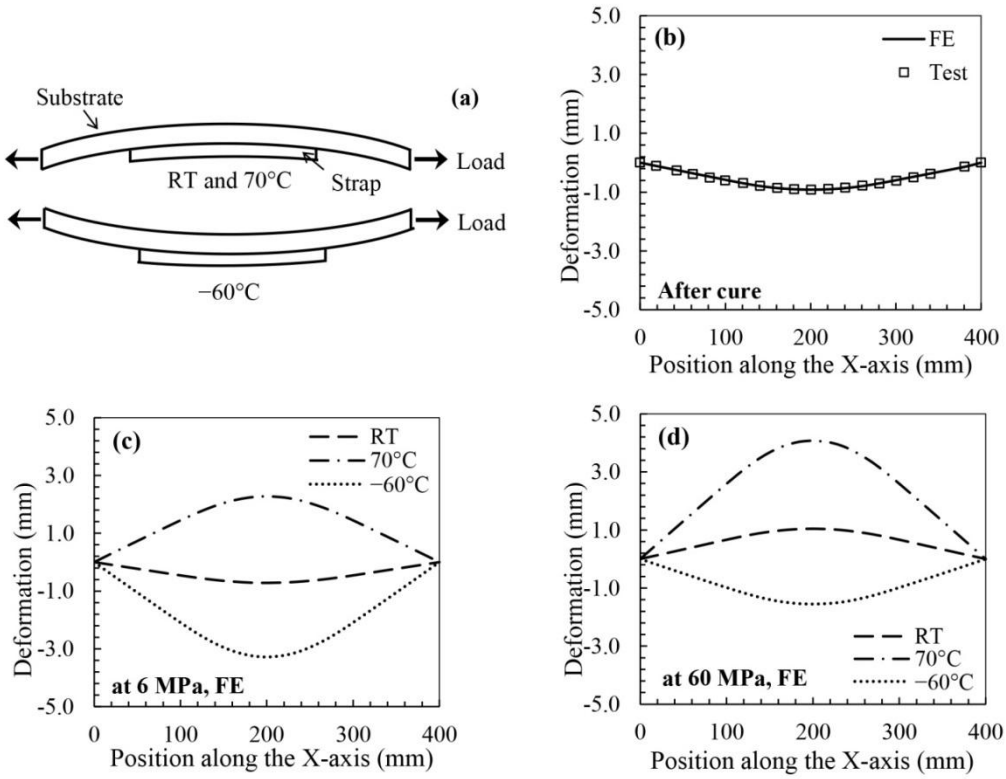

Figure 7: (a) schematic of specimen deformation after strap bonding and subject to loading at different temperatures; (b) FE calculated and test measured deformation after

cure at no load and at room temperature; (c) FE calculated deformation at applied stress 6 MPa; and (d) at applied stress 60 MPa.

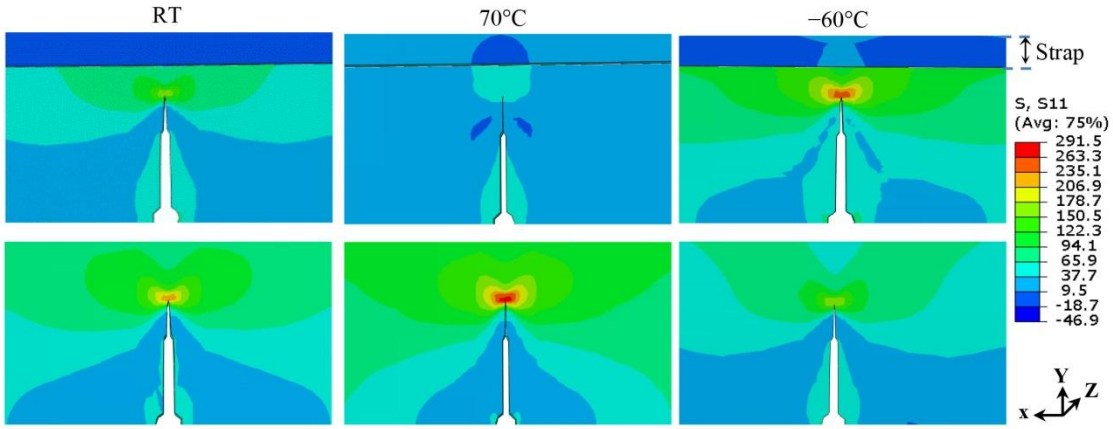

Figure 8: Stresses in the loading (X) direction at 11 mm half crack length loaded to 60 MPa:, reinforced side (top row), unreinforced side (bottom row); left to right, RT, 70°C, −60°C respectively.

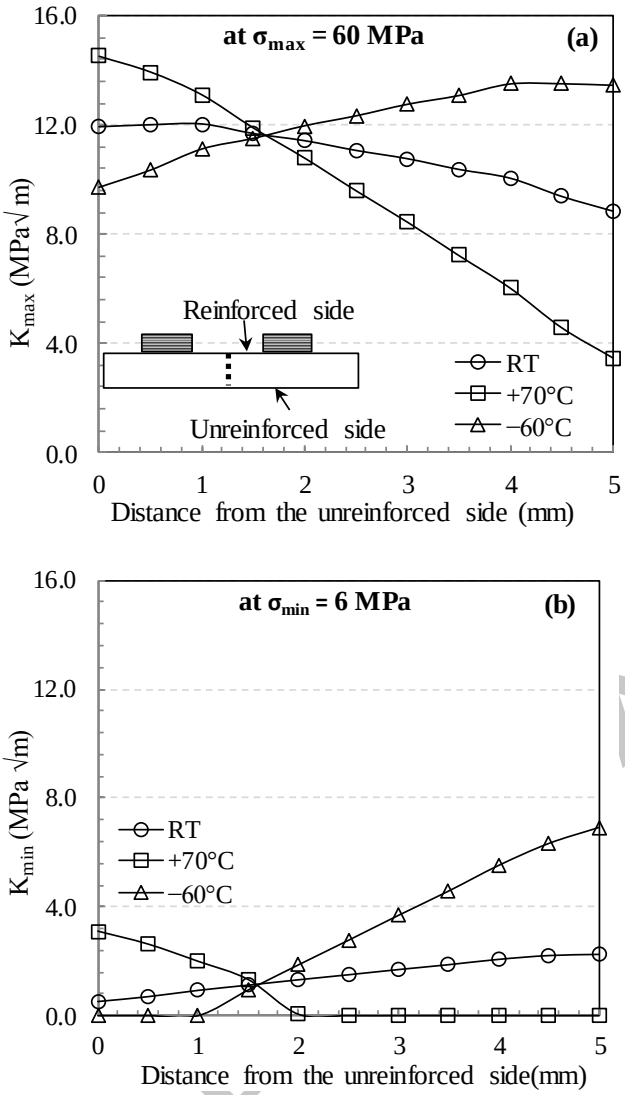

Figure 9: FE analysis of stress intensity factor variation through the substrate thickness for 11 mm half-crack length, (a) K_{max} at 60 MPa applied stress, (b) K_{min} at 6 MPa applied stress

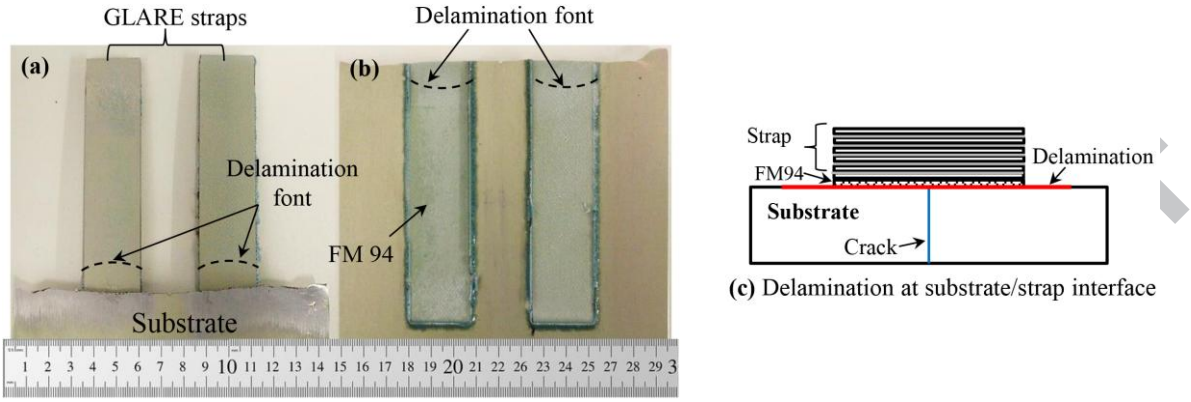

Figure 10: Post-failure images of M(T) specimen tested at 70°C: (a) back face of the substrate and debonded straps showing delamination front at failure, (b) bonded side of the substrate showing adhesive traces on the original strap locations confirming the cohesive failure, with a debond crack running through the FM 94 adhesive, (c) schematic representation of substrate/strap interface delamination.

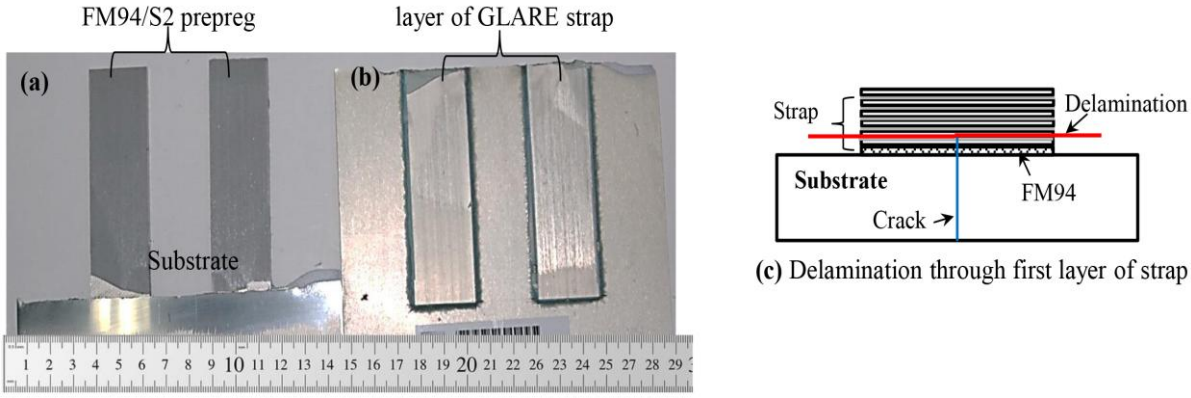

Figure 11: Post-failure image of M(T) specimen tested at −60°C: (a) back face of the substrate and debonded straps showing delamination in GLARE strap, between the first aluminium sheet and the adjacent glass fibre ply, (b) bonded side of the substrate showing delamination and the aluminium sheet intact with the original strap location, (c) Schematic representation of delamination through the first layer of the strap.

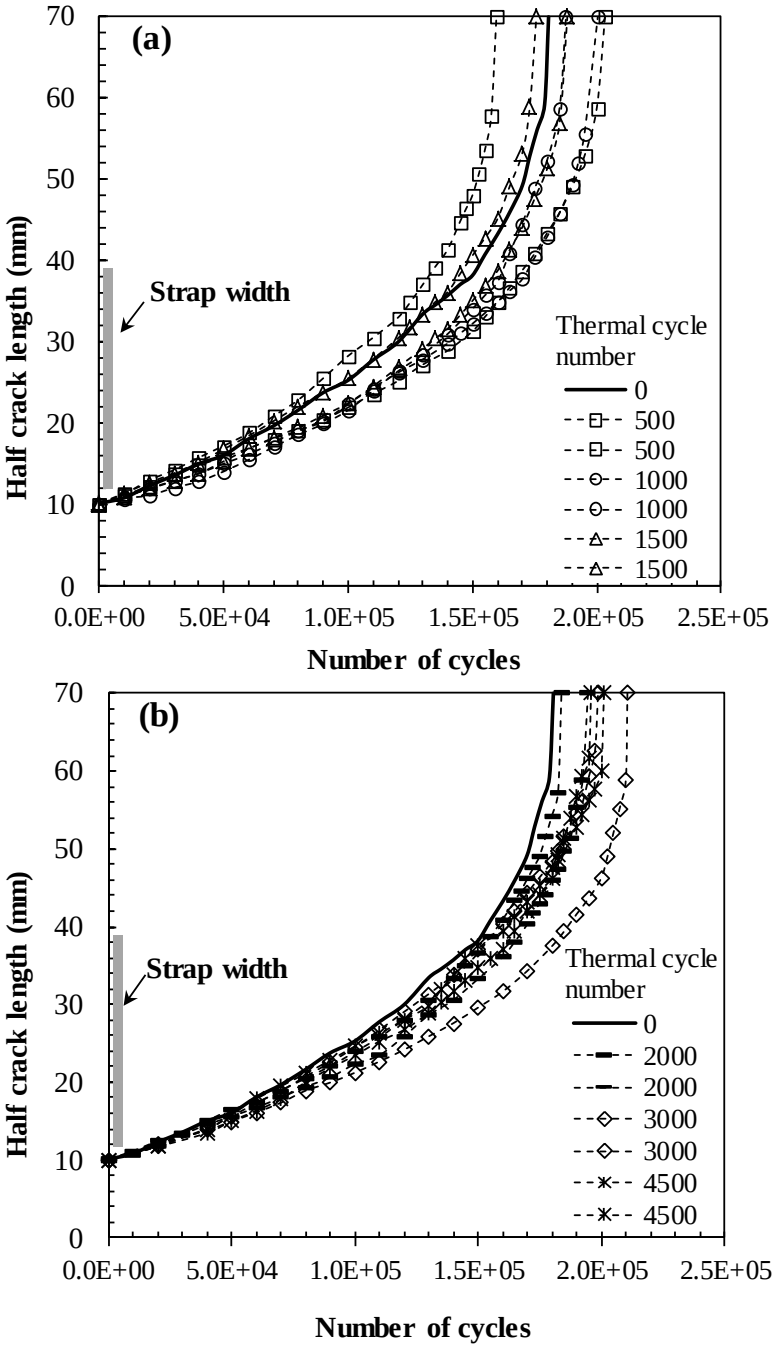

Figure 12: Fatigue crack growth in thermally cycled M(T) specimens (a) 500 - 1500 thermal cycles and (b) 2000 - 4500 thermal cycles prior to fatigue testing.

Table 1: Mechanical properties of materials used in this study

Material	E_1 **(GPa)**	E_2, E_3 **(GPa)**	$\nu_{12} = \nu_{13}$	α_1, α_2 **(** $^{\circ}C^{-1}$**)**	ρ**(g/cm^3)**
AA 2624-T351	73	71	0.33	23.2×10^{-6}	2.77
FM 94	1.90	1.90	0.52	-	1.1

Table 2. Summary of at temperature FCG test programme and results

	Without strap			**With strap**		
Temperature	**RT**	**70°C**	**−60°C**	**RT**	**70°C**	**−60°C**
Average fatigue life (cycles)	147,649	110,728	469,012	177,887	113,320	480,365

Table 3. Paris law constants for 2624-T351 at three temperatures

Paris law constants	**RT**	**70°C**	**−60°C**
***C* (m/cycle)**	3.75×10^{-10}	4.60×10^{-10}	7.30×10^{-11}
n	2.40	2.38	2.62

Table 4. Summary of thermally- cycled test programme and results

Number of thermal cycles	0	500	1000	1500	2000	3000	4500
Average fatigue life (cycles)	175,659	181,433	194,236	181,886	189,250	204,673	198,494

Highlights

- GLARE straps provided considerable reduction to FCG rate at RT.
- At −60°C, baseline FCG life is more than tripled owing to the reduced FCG rate.
- At 70°C, baseline FCG life is shorter owing to greater stress intensity factors.
- Thermal cycling does not impair the performance of BCR tested at RT.